Nuclear hyaluronidase 2 drives alternative splicing of CD44 pre-mRNA to determine profibrotic or antifibrotic cell phenotype

Adam C. Midgley,[1] Sebastian Oltean,[2] Vincent Hascall,[3] Emma L. Woods,[1] Robert Steadman,[1] Aled O. Phillips,[1] Soma Meran[1]*

[1]Wales Kidney Research Unit, Systems Immunity University Research Institute, Division of Infection and Immunity, College of Biomedical and Life Sciences, Cardiff University, Heath Park, CF14 4XN, Cardiff, UK. [2]Institute of Biomedical and Clinical Sciences, University of Exeter Medical School, EX1 2LU, Exeter, UK. [3]Department of Biomedical Engineering, Cleveland Clinic Lerner Research Institute, 9500 Euclid Avenue, Cleveland, OH 44195, USA. *Corresponding author. Email: merans@cf.ac.uk

ABSTRACT

The cell surface protein CD44 is involved in diverse physiological processes, and its aberrant function is linked to various pathologies such as cancer, immune dysregulation, and fibrosis. The diversity of CD44 biological activity is partly conferred by the generation of distinct CD44 isoforms through alternative splicing. We identified an unexpected function for the ubiquitous hyaluronan-degrading enzyme, hyaluronidase 2 (HYAL2), as a regulator of CD44 splicing. Standard CD44 is associated with fibrotic disease, and its production is promoted through serine-arginine–rich (SR) protein–mediated exon exclusion. HYAL2 nuclear translocation was stimulated by bone morphogenetic protein 7, which inhibits the myofibroblast phenotype. Nuclear HYAL2 displaced SR proteins from the spliceosome, thus enabling HYAL2, spliceosome components (U1 and U2 small nuclear ribonucleoproteins), and CD44 pre-mRNA to form a complex. This prevented double-exon splicing and facilitated the inclusion of CD44 exons 11 and 12, which promoted the accumulation of the antifibrotic CD44 isoform CD44v7/8 at the cell surface. These data demonstrate previously undescribed mechanisms regulating CD44 alternative splicing events that are relevant to the regulation of cellular phenotypes in progressive fibrosis.

INTRODUCTION

Fibrosis underlies several organ-specific diseases and contributes to the burden of chronic diseases, such as chronic kidney disease, liver cirrhosis, pulmonary fibrosis, cardiac failure, and degenerative joint disease. Myofibroblasts are the principal effector cells driving fibrosis, and their accumulation in tissues is a fundamental feature of fibrosis (1). These cells are derived from the differentiation of fibroblasts, fibrocytes, or epithelial cells under the influence of circulating profibrotic growth factors such as transforming growth factor–b1 (TGF-b1) (2). Therefore, prevention or reversal of the myofibroblast phenotype is an attractive therapeutic approach to the treatment of fibrotic disease. We have previously shown that this is achievable through stimulation of myofibroblasts with bone morphogenetic protein 7 (BMP7) (3). However, BMP7 itself is not viable for therapy due to its demonstrated ability to promote bone metastasis in osteotropic cancers and its role in promoting ectopic bone formation (4).

Hyaluronan (HA) is a matrix glycosaminoglycan that influences many cellular functions and is implicated in numerous biological processes and disease states. The work from our laboratories demonstrates that establishment and maintenance of the myofibroblast phenotype are dependent on TGF-b1–driven promotion of an HA pericellular matrix, the HA coat (5). CD44 is the principal cell surface HA receptor. It is broadly distributed in tissues and is involved in diverse physiological processes. Its aberrant function is implicated widely in pathology, with key roles in cancer, inflammation, immune dysregulation, vascular disease, fibrosis, and wound healing (6). CD44 is encoded by a single gene consisting of 19 exons and displays considerable protein diversity conferred partly by the ability of these exons to undergo alternative splicing for generating multiple CD44 variant (CD44v) isoforms (7, 8). Exons 1 to 5, 15 to 17, and 19 are constant and present in all alternatively spliced CD44 mRNA species. These exons encode the extracellular N-terminal domain, the transmembrane domain, and the cytoplasmic region, all of which are present in every CD44 isoform. The presence of exons 6 to 14 varies between isoforms, resulting in the multitude of CD44v presently documented. Exon 18 is removed before translation inmost isoforms due to its inclusion of an early stop codon. One isoform described to contain exon 18 is a small, truncated form of CD44 with no intracellular signaling domain, the function of which remains unclear (9). Standard CD44 (CD44s) is the most abundant CD44 isoform with a predicted molecular mass of 85 to 90 kDa. CD44s only contains regions encoded by exons 1 to 5, 15 to 17, and 19. All other variants have this overall pattern but include additional amino acid sequences derived from various combinations of exons 6 to14. These sequences form the extracellular stem structure, resulting in receptor variants of different sizes (Fig. 1, A to B). TGF-b1–driven HA coat assembly and myofibroblast differentiation is dependent on the 85- to 90-kDa CD44s, which is processed into a 347 amino acid sequence that colocalizes with the epidermal growth factor receptor (EGFR) within cholesterol-rich lipid rafts (10). By contrast, BMP7-driven HA coat dissolution and prevention or reversal of the myofibroblast phenotype depend on the presence of the 190-kDa variant isoform CD44v7/8, which is processed into a 424 amino acid–containing protein and so named because this isoform is encoded from CD44 pre-mRNA that contains the two variable region exons, 11 and 12 (Fig. 1C). These exons encode an extracellular stem region, which is thought to convey an additional glycosylation site

and additional function to the CD44v7/8 protein (3). Factors that govern the production of the pro- or antifibrotic CD44 isoforms are unclear; therefore, we investigated the regulation of CD44 alternative splicing under antifibrotic conditions. Here, we present a mechanism that controls CD44 alternative splicing events relevant to the determination of cell phenotype.

The breakdown of HA is mediated by the hyaluronidase (HYAL) group of enzymes. HYAL1 and HYAL2 are the most abundant HYALs in vertebrates. HYAL2 is present in many tissues, and its biological importance has been demonstrated in studies of Hyal2 knockout mice, which display skeletal abnormalities, cardiopulmonary dysfunction, hematological anomalies, and exacerbated renal inflammation and fibrosis (11, 12). Previously, HYAL2 has been identified within lysosomes, wherein the acidic environment is optimal for HYAL activity. In addition, HYAL2 has been identified as a cell membrane-anchored protein, where it only has weak enzymatic activity (13–15). Several reports also indicate that a large proportion of HYAL2 in tissues may be enzymatically inactive, so its cellular function in context of cellular localization is unclear (16–18). Here, we identify an unexpected nonenzymatic function for HYAL2 that can potentially explain its broad biological effects. We identify HYAL2 as a key regulator of pre-mRNA splicing that dictates the production of CD44v isoforms.

RESULTS

Fluorescent bichromatic minigene reporters indicate BMP7-regulated CD44 alterative splicing

The CD44s and CD44v7/8 proteins are produced from divergent transcripts that are generated by alternative splicing of theCD44 pre-mRNA (Fig. 1, A to C). In addition to the standard exons (exons 1 to 5, 15 to 17, and 19), the CD44v7 variant isoform includes exon 11 [132 base pairs (bp)], and the CD44v8 isoform includes exon 12 (102 bp), whereas the CD44v7/8 variant isoform includes both exons 11 and 12 (234 bp). Therefore, to better understand alternative splicing resulting in CD44v7/8, we developed two fluorescent bichromatic minigene reporters to investigate splicing activity surrounding the variable exons. The two minigene reporters were used to determine what factors influenced induction of CD44s versus CD44v7 or CD44v8 (fig. S1, A and B). The minigene reporter plasmids contain a bichromatic reporter that produces either red fluorescent protein (dsRED) or enhanced green fluorescent protein (EGFP), depending on exon inclusion or exclusion, respectively. These pRG6 minigenes use the original construct backbone developed by Orengo et al. (19). Exon 11 and flanking introns 10 and 11 (pRG6-CD44v7) or exon 12 and flanking introns 11 and 12 (pRG6-CD44v8) were cloned into the minigene reporters. The presence of red fluorescence indicates the inclusion of the alternatively expressed exon 11 (pRG6-CD44v7) or exon 12 (pRG6-CD44v8), indicating conditions that favor increased CD44v7/8 production. Green fluorescence indicates the exclusion of the exons, indicating conditions that favor CD44s production. Stimulating proximal tubular epithelial cell (PTEC) (HK-2) cells expressing either pRG6-CD44v7 or pRG6-CD44v8 with BMP7 attenuated green fluorescence and increased red fluorescence (fig. S1, C and D), confirming BMP7 as an important inducer of alternative splicing that favors CD44v7/8 production.

CD44s expression is dependent on SRSF2 and SRSF5

An in silico analysis of intronic sequences surrounding exons that are included in CD44v7 and v8 revealed recognition sites for SR splicing factor (SRSF) proteins (fig. S2). Threshold scores for SRSF2 and SRSF5 binding sites were prominent, suggesting a role for these proteins in CD44 alternative splicing (tables S1 and S2). We transfected PTEC (HK-2) lines stably expressing the reporter pRG6-CD44v7 or pRG6-CD44v8 with constructs encoding small interfering RNAs (siRNAs) directed against SRSF2 or SRSF5 (Fig. 2,AandB). Protein knockdown was also confirmed (fig. S3). Cells transfected with scrambled controls demonstrated only green fluorescence, indicating that exons 11 or 12were spliced out to generate CD44v7 or CD44v8, respectively. Scrambled controls stimulated with BMP7 showed reduced green and increased red fluorescence, indicating appropriate inclusion of exon 11 (CD44v7) or exon 12 (CD44v8) and suggesting enhanced CD44v7/8 expression. SRSF2 knockdown in unstimulated cells increased red and attenuated green fluorescence, mimicking the effects of BMP7. This effect was more pronounced with knockdown of SRSF5 in unstimulated cells, which fully mimicked BMP7 conditions, abrogating green and promoting red fluorescence. Thus, both splice factors were required for exons 11 and 12 skipping; however, the effect of SRSF5 knockdown was more pronounced. BMP7 stimulation of cells with SRSF2 knockdown caused a shift in fluorescence that did not occur in BMP7-stimulated cells with SRSF5 knockdown, which also highlighted the particular importance of SRSF5. We assessed the direct effects on CD44s and CD44v7/8 mRNA expression by real-time quantitative reverse transcription polymerase chain reaction (qRT-PCR). Successful SRSF2 mRNA knockdown was verified (Fig. 2C). CD44s mRNA expression showed no significant attenuation after SRSF2 knockdown (Fig. 2D), we found that SRSF2 knockdown enhanced CD44v7/8 mRNA expression, implicating SRSF2 in promoting CD44s splicing (Fig. 2E). After verifying SRSF5 knockdown (Fig. 2F), we found that SRSF5 knockdown significantly attenuated CD44s mRNA expression (Fig. 2G) and enhanced CD44v7/8 expression (Fig. 2H). These data indicate a role for SRSF2 and SRSF5 in

preventing alternative splicing to generate CD44v7/8 and a role for SRSF5 in driving CD44s mRNA expression.

Nuclear HYAL2 interacts with CD44 pre-mRNA to promote CD44v7/8 alternative splicing

We previously demonstrated that BMP7 increased HYAL2 mRNA expression and that HYAL2 was critical in mediating BMP7-driven prevention or reversal of the myofibroblast phenotype (3). Here, we investigated the potential role of HYAL2 on the regulation of CD44 alternative splicing. We first determined whether BMP7 influenced HYAL2 cellular localization. Confocal microscopy demonstrated increased nuclear accumulation of HYAL2 in primary human lung fibroblasts, in response to BMP7 treatment (Fig. 3A). This was confirmed by immunoblotting of nuclear extracts, which showed reduced cytoplasmic and increased nuclear HYAL2 protein after BMP7 treatment (Fig. 3, B and C). Nuclear HYAL2 exhibited a slightly reduced molecular weight compared to cytoplasmic HYAL2 (~4 to 5 kDa smaller), suggesting that the protein undergoes cytoplasmic cleavage before nuclear translocation. siRNA-mediated knockdown of HYAL2 strongly reduced, but did not entirely eliminate, both cytoplasmic and nuclear HYAL2 abundance. Subsequent RNA immunoprecipitation (RIP) assays using antibodies directed against HYAL2 were used to assess the potential of HYAL2 to bind to and interact with mRNA or pre-mRNA. RIP assays revealed binding interactions between HYAL2 and CD44 intron 10 under all conditions tested and betweenHYAL2andCD44 intron 12 afterBMP7stimulation (Fig. 3D). These intronic sequences flank CD44 exons 11 and 12, which are included in the CD44v7 and CD44v8 pre-mRNA transcripts, respectively, in addition to the CD44s exons.

To determine the effects ofHYAL2 on CD44v7/8 mRNA expression and protein abundance, we used siRNAs to knock downHYAL2 (Fig. 4A) in primary human lung fibroblasts and measured the abundance of the transcripts and proteins by qRT-PCR, Western blotting, and fluorescence microscopy. HYAL2 knockdown induced a small increase in CD44s mRNA expression in untreated fibroblasts (Fig. 4B) and attenuated both basal and BMP7-driven expression of CD44v7/8 (Fig. 4C), indicating that, in the absence of HYAL2, CD44 pre-mRNA did not undergo alternative splicing to generate CD44v7/8 mRNA. At the protein level, HYAL2 knockdown reduced the abundance of CD44v7/8 but did not influence the abundance of CD44s (Fig. 4, D and E). Knocking down HYAL2 in PTEC (HK-2) lines, stably expressing the minigene reporter pRG6-CD44v7 or pRG6-CD44v8 (Fig. 4F), increased CD44s expression in untransfected, untreated cells and in pRG6-CD44v7–expressing cells that were treated with BMP7 (Fig. 4G). HYAL2 knockdown also prevented the BMP7-induced increase in CD44v7/8 expression in untransfected, pRG6-CD44v7–expressing, and pRG6-CD44v8–expressing cells (Fig. 4H). Fluorescence microscopy verified these results. After HYAL2 knockdown, BMP7 treatment no longer promoted the shift from green fluorescence to red. Instead, HYAL2 knockdown mimicked the results seen in unstimulated cells (Fig. 4, I and J), confirming HYAL2 as a critical regulator of CD44v7/8 alternative splicing.

To identify proteins that interact with HYAL2, we performed mass spectrometry (MS) on proteins that coimmunoprecipiated with HYAL2 from primary human lung fibroblast nuclear extracts. We identified 13 candidate proteins that interacted with nuclearHYAL2 and could potentially function with HYAL2 to affect CD44 alternative splicing (table S3). These candidates included proteins involved in nuclear trafficking (nuclear pore complex trafficking protein and spectrin), alternative splicing (zinc finger matrin-type protein 2 and RNA binding protein), and DNA or RNA processing (elongation factor of translation and translation initiation factors). Identification of these putative binding partners suggests that HYAL2 might influence splicing of other target genes in addition to CD44. However, we detected no association between HYAL2 and SRSF proteins using this method. In silico analysis of theHYAL2 peptide sequence demonstrated a putative bipartite nuclear localization signal (NLS) motif 34 amino acids downstream from the designated HYAL2 active site (table S4). This suggests that HYAL2 may undergo nuclear trafficking by association with importins (20). Furthermore, four putative binding sites for DNA and RNA nucleotide sequences were located downstream of the NLS motif of HYAL2, and one was located within the HYAL2 EGF-like domain, near the C terminus.

HYAL2 displaces SRSF5 from CD44 pre-mRNA and the early spliceosome, thus preventing SRSF5-spliceosome–mediated exon 11 and exon 12 exclusion

HYAL2 and SRSF proteins were both implicated in CD44 alternative splicing but with opposing effects. Direct interactions between HYAL2 and SRSFs were directly investigated, but coimmunoprecipitation demonstrated no binding between HYAL2 and SRSF2 or SRSF5 (Fig. 5A). We performed RIP assays in primary human lung fibroblasts using antibodies directed against SRSF2 or SRSF5 in the presence or absence of siRNAtargetingHYAL2. RIP assays demonstrated no association of SRSF2 with CD44 pre-mRNA, because the enrichment was comparable to RIP negative control immunoglobulin G (IgG) (fig. S4), which suggested that the role of SRSF2 in CD44 alternative splicing was not through direct SRSF2-CD44 pre-mRNA associations. By contrast, SRSF5 exhibited high fold enrichment and associations with CD44 introns 10 and 12 in unstimulated cells, and BMP7 stimulation attenuated these interactions.

HYAL2 knockdown prevented BMP7 treatment from attenuating the interactions between SRSF5 and CD44 introns, indicating that the BMP7 response was HYAL2-dependent (Fig. 5B). Thus, HYAL2 appeared to displace SRSF5 from CD44 intron 12 splice sites, thereby preventing SRSF5-mediated exons 11 and 12 skipping. Subsequent experiments demonstrated that HYAL2 knockdown increased SRSF2 and SRSF5 mRNA expression (Fig. 5, C and D), suggesting a role for HYAL2 in the transcriptional repression of these splicing factors.

In silico analysis of intronic sequences surrounding exons 11 and 12 identified 3′ and 5′ U2-acceptor sites on introns 10, 11, and 12 as regions of putative spliceosome activity (fig. S2). Consequently, we performed RIP assays using antibodies recognizing HYAL2, SRSF2, or SRSF5 to assess the association of these proteins with several spliceosome components: U1, U2, U4, and U6 small nuclear RNAs (snRNAs). BMP7 promoted strong interactions between HYAL2 and the U1 and U2 snRNAs (U1/U2), which comprise the early spliceosome (Fig. 5E). HYAL2 knockdown significantly enhanced the association between SRSF2 and U1/U2 and between SRSF2 and U4 and U6 (U4/U6), suggesting HYAL2 involvement in the regulation of SRSF2-spliceosome interactions (Fig. 5F). Similarly, SRSF5 demonstrated strong interactions with the snRNA components of early (U1/U2) and mature (U4/U6) spliceosomes in unstimulated cells, and BMP7 significantly reduced these associations (Fig. 5G). HYAL2 knockdown prevented the BMP7-mediated attenuation of SRSF5-spliceosome interactions, indicating that HYAL2 was essential for SRSF5-spliceosome dissociation. Hence, HYAL2 prevents mature spliceosome formation and splicing initiation, thus favoring CD44v7/8 expression. In concert, our data support a model wherein SRSF2 and SRSF5 bind to intronic regions of CD44 pre-mRNAs to promote variant exon exclusion, thus enhancing CD44s expression. HYAL2 displaces SRSF2 and SRSF5 from CD44 pre-mRNA intronic regions and from the spliceosome complex to promote exons 11 or 12 inclusion, thus enhancing CD44v7/8 mRNA expression and protein production (Fig. 6, A to C).

DISCUSSION

The roles of CD44v isoforms have been widely studied in cancer, with different isoforms shown to have distinct and sometimes opposing functions (7). However, the relevance of these isoforms to the promotion and prevention of fibrotic disorders has only begun to be appreciated. An understanding of cellular and molecular mechanisms that regulate the switch from deleterious (profibrotic) to protective (antifibrotic) CD44vs may therefore be an important determinant of fibrosis outcomes. Previous studies investigated regulators of CD44 alternative splicing in the context of cancer biology, but limited information is available regarding CD44 alternative splicing in fibrosis. Induction of type III epithelial-mesenchymal transition (EMT) in cancer, which is similar to type II EMT in fibrosis, is associated with a shift in CD44 isoforms from variants to the standard (CD44s) isoform. Epithelial splicing regulatory proteins, argonaute-mediated histone modifications, Src associated mitosis 68 kDa (Sam68), and transformer 2 b homolog have been identified as regulators of CD44 splicing (8, 21, 22), mainly in cancers. In addition, Sam68 is activated by Ras and downstream of Ras and extracellular signal–regulated kinases 1 and 2 (ERK1/2) signaling, and influences alternative splicing to result in increased expression of CD44v5, in which exon 9 is included (8). Ras and ERK1/2 are also important regulators of profibrotic cellular signaling pathways, suggesting that CD44v5, in addition to CD44s, may favor the generation of profibrotic cellular phenotypes. Here, we show that HYAL2, SRSF2, and SRSF5 play integral roles in controlling cell systems relevant to fibrosis and type II EMT by acting as CD44 splicing regulators. Although SRSF proteins are commonly thought to enhance exon inclusion, the literature indicates that their position relative to a 5′ splice site determines whether they activate or repress splicing (23).

The presence of the enzyme HYAL2 in the nucleus was unexpectedly able to counteract the effects of SRSF5 in CD44 pre-mRNA splicing and played a key role in regulating the production of SRSF2 and its interactions with CD44 pre-mRNA. All HYAL2 activities have been previously ascribed to its role in HA catabolism. Murine studies demonstrated that extracellular HA accumulated in Hyal2-null tissues, indicating a clear role for HYAL2 in HA degradation (24). However, HYAL2 exhibits very low enzymatic activity compared to other HYALs and requires a pH of 3.8 for optimal activity (25). Therefore, why an enzyme that functions optimally in acidic pH should be present in tissues with higher pH values or what the purpose of nonenzymatically active HYAL2 may be has been unclear and raised the possibility of noncatabolic functions for this protein. It was proposed that cofactors mightmodulateHYAL2 activity to convert it into a more active enzyme at higher pH. It has been reported that the ability of HYAL2 to promote acidification of the cellular microenvironment requires the presence of the Na^+/H^+ exchanger NHE1 (26). However, there are reports that HYAL2 has additional functions beyond its role in HA catabolism. Duterme et al. (17) found that HYAL2 functions as a co-receptor forCD44, Liu et al. (18) identifiedHYAL2 as a viral cell entry receptor, and Hsu et al. (27) showed that cell surface HYAL2 formed a complex with TGF-b1 and WW domain–containing oxidoreductase (WWOX). In relevance to fibrosis, Colombaro et al. (12) demonstrated that knocking out Hyal2 in mice exacerbates renal fibrosis in response to ischaemia-reperfusion injury. In previous studies, we have shown that cells deficient in HYAL2 are no longer resistant to BMP7-driven prevention and reversal of the myofibroblast phenotype (3). In extension of our previous findings, this study

presents a previously undiscovered nonenzymatic role for HYAL2 in regulating alternative splicing that is relevant to the cell biology of fibrosis.

The data presented here support a model wherein SRSF5 binds to putative 3′ and 5′ intronic splicing sites within introns 10 and 11 of CD44 pre-mRNA (Fig. 6A). SRSF5 binding to these splice sites recruits snRNPs, leading to the formation of mature spliceosomes (U1/U2 and U4/U6.U5). This promotes variant exon exclusion by means of double exon skipping alternative splicing. SRSF2 does not bind to this region of CD44 pre-mRNA but associates with U1/U2 snRNPs and, according to previous literature (28), functions in promoting the efficacy of U1/U2 splicing initiation and mature tri-snRNP (U4/U6.U5) binding, thereby promoting the production of CD44s transcripts that are translated into CD44sprotein (Fig. 6B). The presence of CD44s on the cell surface promotes HA coat maintenance, which facilitates myofibroblast differentiation. BMP7 stimulation promotes translocation of HYAL2 to the nucleus, where it displaces SRSF5 from the early spliceosome (U1/U2) and prevents the SRSF5-mediated formation of mature spliceosomes. HYAL2 also acts at the intronic splice site, where it prevents SRSF5 from binding to intron 12 of theCD44 pre-mRNA. This impairs recruitment of the spliceosome to CD44 pre-mRNA, preventing the double-exon skipping splicing event and resulting in the inclusion of exons 11 and 12 (Fig. 6C). CD44v7/8 is subsequently produced and present at the cell surface, where it promotes HA coat internalization, thus blocking myofibroblast differentiation. Although the data demonstrate a clear mechanism for the displacement of SRSF5 by HYAL2, the influence of HYAL2 on SRSF2 is less clear. We postulate that HYAL2 inhibits SRSF2 transcription, thus favoring the production of CD44v7/8 by reducing alternative splicing activity through attenuation of spliceosome recruitment to the CD44 pre-mRNA, specifically around exons 11 and 12. Therefore, stimuli resulting in HYAL2 attenuation would reduce nuclear HYAL2, enhance SRSF2 abundance, and lead to its increased availability and interactions with early and mature spliceosome snRNPs, promoting CD44s expression.

HYAL2 functionality is considerably more complex than was initially envisaged after its discovery as a catabolic enzyme involved in HA degradation. Although we have not directly tested whether the catalytic activity of HYAL2 is dispensable in influencing CD44 splicing, given that HYAL's only known substrate is HA, any function dependent on catalytic activity would likely require the presence of HA within the nucleus. Although this report demonstrates an important role for HYAL2 in CD44 alternative splicing, the presence of nuclear HYAL2 and its interaction with regulators of DNA and RNA processing suggest that HYAL2 may have as-yet-undiscovered roles in regulation of gene expression.

FIGURES

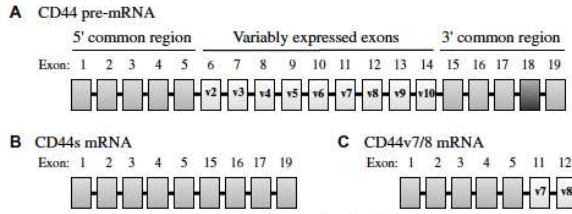

Fig. 1. Schematic of CD44 pre-mRNA and alternatively spliced CD44s and CD44v7/8 mRNAs. (**A**) Intron-exon structure of CD44 pre-mRNA. The 5′ common region exons 1 to 5 and 3′ common region exons 15 to 17 and 19 are present in all *CD44* splice variants. Exon 18 is removed before translation, and exons 6 to 14 are differentially expressed in different *CD44* variant isoforms. (**B**) *CD44s* mRNA contains only the common exons 1 to 5, 15 to 17, and 19. All variably expressed exons are removed from this isoform by splicing. (**C**) The *CD44v7/8* mRNA contains the same common region exons as *CD44s* plus the addition of the variably expressed exons 11 and 12. *CD44v7* mRNA contains the same common region exons as *CD44s* plus the variably expressed exon 11. *CD44v8* mRNA contains the same common region exons as *CD44s* plus the variably expressed exon 12. Exons 11 and 12 encode an extracellular stem region.

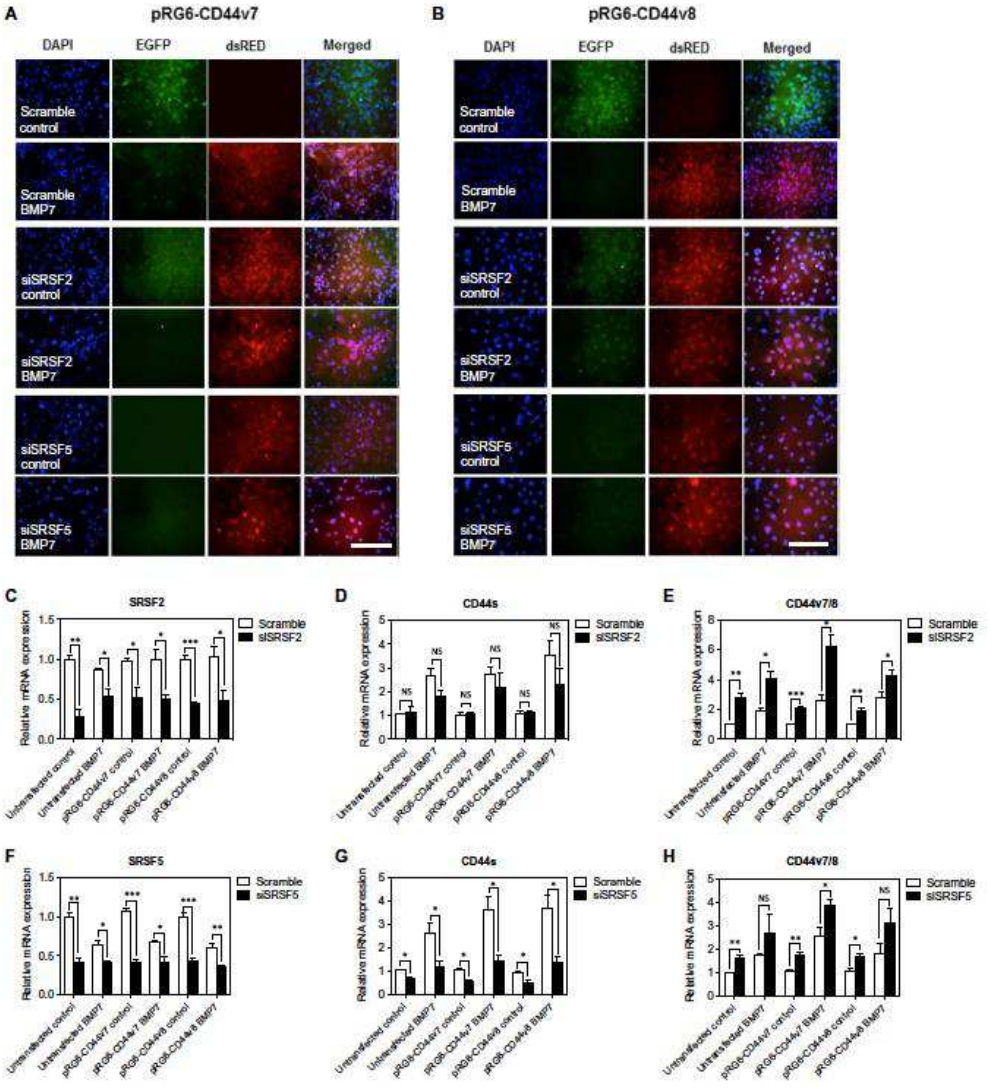

Fig. 2. *CD44s* expression is dependent on the splicing regulators SRSF2 and SRSF5. Fluorescence microscopy showing enhanced green fluorescent protein (EGFP) or red fluorescent protein (dsRED) expression in proximal tubular epithelial cell (PTEC) (HK-2) cell lines stably expressing (**A**) pRG6-CD44v7 or (**B**) pRG6-CD44v8 after transfection with a scrambled small interfering RNA (siRNA) or scrambled siRNAs directed against *SRSF2* or *SRSF5* in the presence or absence of bone morphogenetic protein 7 (BMP7). Scale bar, 100 μm. (**C** to **H**) Expression of *SRSF2*, *CD44s*, and *CD44v7/8* in untransfected PTECs and in PTEC cell lines stably expressing pRG6-CD44v7 or pRG6-CD44v8 and cotransfected with constructs encoding scrambled siRNAs (white bars) or siRNAs directed against *SRSF2* or *SRSF5* (black bars). Real-time quantitative reverse transcription polymerase chain reaction (qRT-PCR) showing abundance of (**C**) *SRSF2*, (**D**) *CD44s*, and (**E**) *CD44v7/8* mRNAs in cells transfected with siRNA targeting *SRSF2* (siSRSF2). qRT-PCR showing abundance of (**F**) *SRSF5*, (**G**) *CD44s*, and (**H**) *CD44v7/8* mRNAs in cells transfected with siRNA targeting *SRSF5* (siSRSF5). All data are means ± SE of three independent experiments ($n = 3$). Statistical analysis is shown as $^{*}P \leq 0.05$, $^{**}P \leq 0.01$, and $^{***}P \leq 0.001$, as determined by Tukey's posttest. NS, nonsignificant.

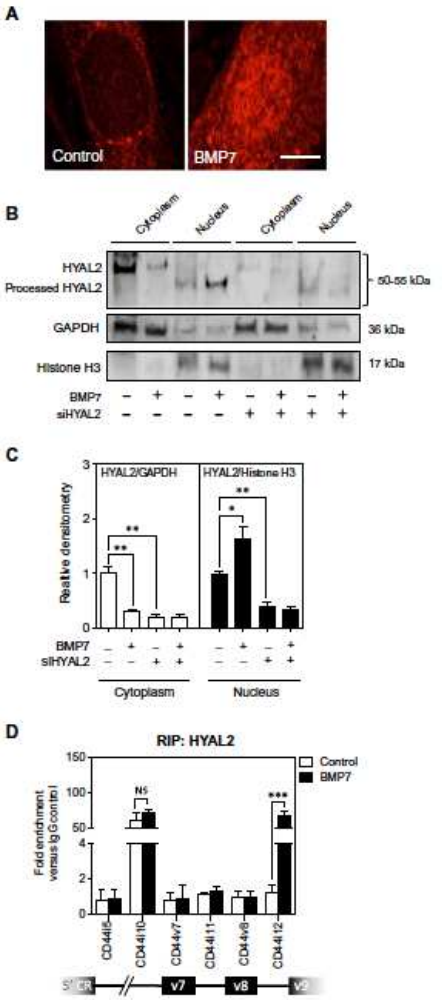

Fig. 3. BMP7 promotes HYAL2 nuclear translocation and binding to *CD44* pre-mRNA. (**A**) Confocal microscopy images showing hyaluronidase 2 (HYAL2) accumulation in growth-arrested primary human lung fibroblasts after BMP7 stimulation. Scale bar, 5 μm. (**B**) Western blots showing HYAL2 protein abundance in cytoplasmic and nuclear fractions with glyceraldehyde-3-phosphate dehydrogenase (GAPDH) and histone H3 as loading controls. The cells were transfected with a construct encoding a siRNA targeting HYAL2 (siHYAL2^{+}) or scrambled control siRNA (siHYAL2^{-}), as indicated, before growth arrest and BMP7 treatment. (**C**) Densitometric analysis of Western blots in (B). (**D**) RNA immunoprecipitation (RIP) using an antibody directed against HYAL2 followed by qRT-PCR to detect the indicated regions of *CD44* transcripts. Intronic regions, CD44i$_{\chi}$; exonic regions, CD44v$_{\chi}$; χ, intron or exon number. Images and blots are representative of three independent experiments using fibroblasts; similar results were obtained using PTEC (HK-2) cells. Data are means ± SE of three independent experiments ($n = 3$). Statistical analysis is shown as $^{*}P \leq 0.05$, $^{**}P \leq 0.01$, and $^{***}P \leq 0.001$, as determined by Tukey's posttest.

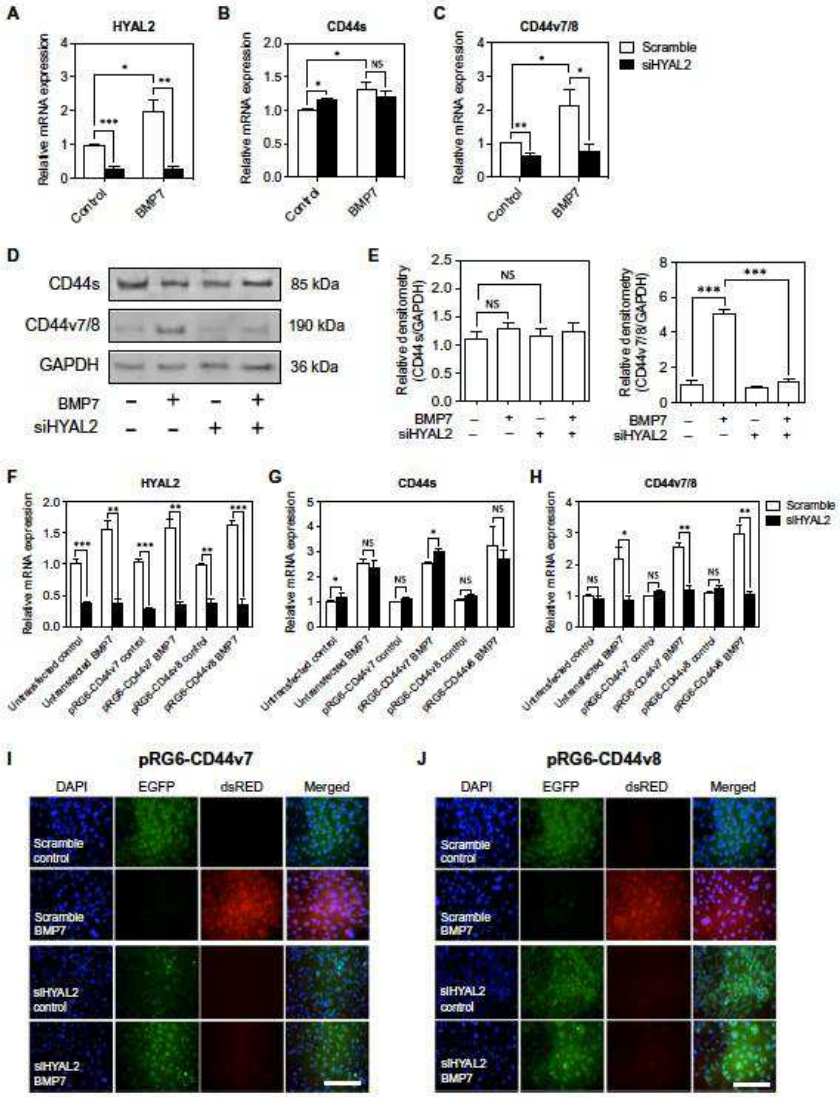

Fig. 4. HYAL2 is a critical regulator of CD44v7/8 alternative splicing. Expression of (**A**) *HYAL2*, (**B**) *CD44s*, and (**C**) *CD44v7/8* by qRT-PCR after BMP7 treatment of primary human lung fibroblasts transfected with scrambled siRNAs (white bars) or siRNAs directed against HYAL2 (siHYAL2, black bars). (**D**) Western blot showing CD44s (standard CD44) and CD44v7/8 protein abundance after BMP7 treatment of primary human lung fibroblasts expressing siHYAL2. GAPDH was used as a loading control. (**E**) Densitometric analysis of Western blot in (C). (**F** to **H**) qRT-PCR showing expression of (F) *HYAL2*, (G) *CD44s*, and (H) *CD44v7/8* in PTEC (HK-2) cell lines stably expressing pRG6-CD44v7 or pRG6-CD44v8 and transfected with scrambled siRNAs (white bars) or siRNAs targeting HYAL2 (siHYAL2, black bars). (**I** and **J**) Fluorescence microscopy showing EGFP or dsRED in cells expressing (I) pRG6-CD44v7 or (J) pRG6-CD44v8. Scale bars, 100 μm. Images, blots, and graphs are representative of three experiments. Data are means ± SE of three independent experiments ($n = 3$). Statistical analysis is shown as $^{*}P \leq 0.05$, $^{**}P \leq 0.01$, and $^{***}P \leq 0.001$, as determined by Tukey's posttest.

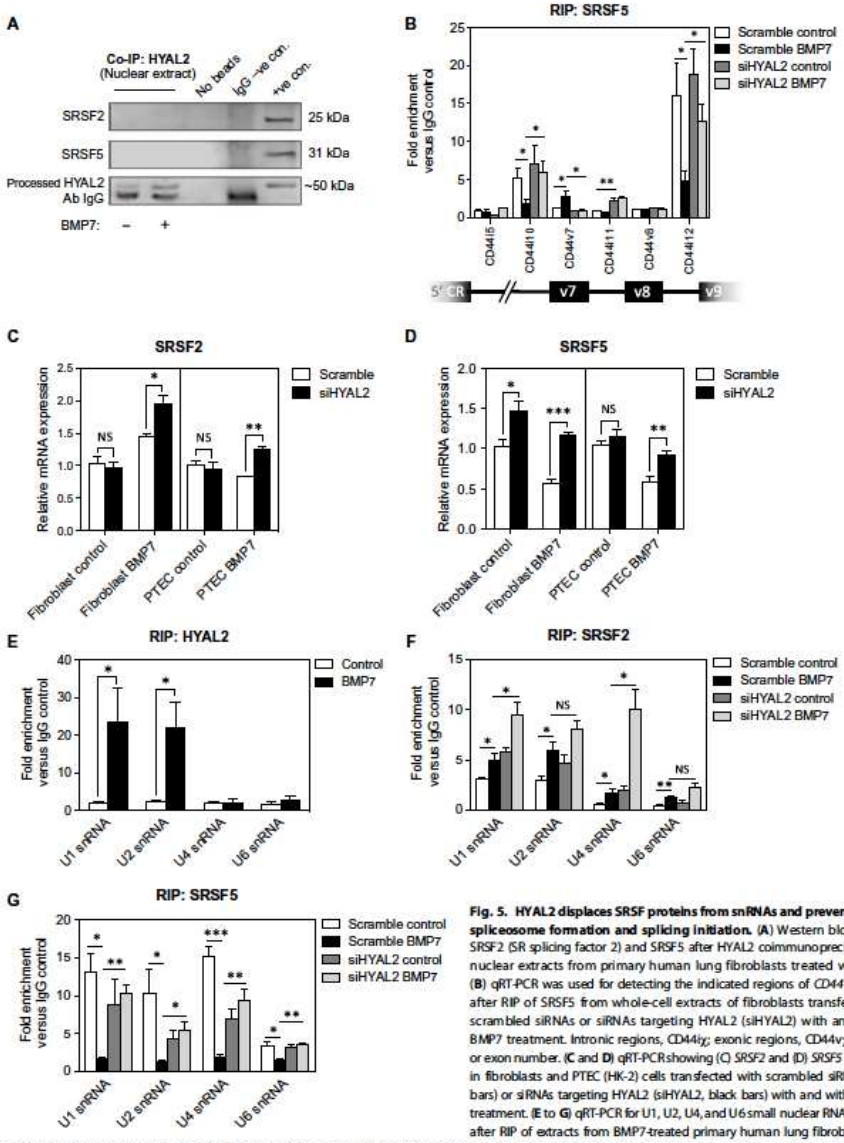

Fig. 5. HYAL2 displaces SRSF proteins from snRNAs and prevents mature spliceosome formation and splicing initiation. (**A**) Western blot showing SRSF2 (SR splicing factor 2) and SRSF5 after HYAL2 coimmunoprecipitation of nuclear extracts from primary human lung fibroblasts treated with BMP7. (**B**) qRT-PCR was used for detecting the indicated regions of *CD44* transcripts after RIP of SRSF5 from whole-cell extracts of fibroblasts transfected with scrambled siRNAs or siRNAs targeting HYAL2 (siHYAL2) with and without BMP7 treatment. Intronic regions, CD44i*χ*; exonic regions, CD44v*χ*; *χ*, intron or exon number. (**C** and **D**) qRT-PCR showing (C) *SRSF2* and (D) *SRSF5* expression in fibroblasts and PTEC (HK-2) cells transfected with scrambled siRNAs (white bars) or siRNAs targeting HYAL2 (siHYAL2, black bars) with and without BMP7 treatment. (**E** to **G**) qRT-PCR for U1, U2, U4, and U6 small nuclear RNAs (snRNAs) after RIP of extracts from BMP7-treated primary human lung fibroblasts using antibodies directed against (E) HYAL2, (F) SRSF2, or (G) SRSF5. Blots represent three independent experiments using fibroblasts; similar results were obtained using PTEC (HK-2) cells. Data are means ± SE of three independent experiments ($n = 3$). Statistical analysis is shown as *$P \leq 0.05$, **$P \leq 0.01$, and ***$P \leq 0.001$, as determined by Tukey's posttest.

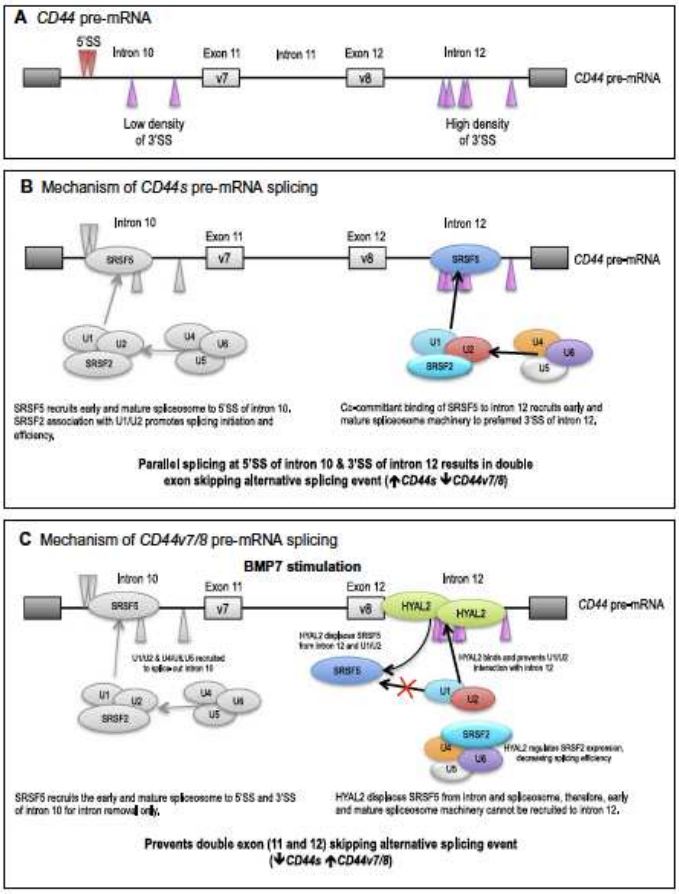

Fig. 6. Model for alternative splicing that generates profibrotic and antifibrotic isoforms of CD44. (**A**) Schematic of *CD44* pre-mRNA from intron 10 to intron 12, indicating putative 5′ splice sites (5′SS; red triangles) and 3′SS (pink triangles). The high density of 3′SS within intron 12 suggests preferential binding of the spliceosome to this intron under basal conditions, favoring splicing activity at these sites. *CD44v7/8* pre-mRNA includes exon 11 (v7) and exon 12 (v8). (**B**) Mechanism of *CD44s* pre-mRNA splicing. Under basal conditions, there is preference for splicing that favors *CD44s* expression. Binding of SRSF5 to introns 10 and 12 recruits early spliceosomes (U1/U2) to the 5′SS of intron 10 and the 3′SS of intron 12. SRSF2 facilitates the activity of early spliceosomes. Subsequent recruitment of the mature spliceosome machinery (U4/U6. U5) results in a double-exon-skipping alternative splicing event, wherein introns 10 and 12 are spliced out simultaneously, and exons 11 and 12 and intron 11 are removed. This generates the *CD44s* transcript, which lacks both exons 11 and 12. Production of CD44s allows establishment of the myofibroblast-stabilizing hyaluronan (HA) coat and signaling through epidermal growth factor receptor (EGFR) after transforming growth factor–β1 (TGF-β1) stimulation. (**C**) Mechanism of *CD44v7/8* alternative splicing. After BMP7 stimulation, there is preference for splicing to increase *CD44v7/8* expression. HYAL2 displaces SRSF5 that is bound to the 3′SSs in intron 12 of the *CD44* pre-mRNA. HYAL2 concomitantly displaces SRSF5 from U1/U2, preventing initiation of splicing at intron 12. HYAL2 also attenuates *SRSF2* and *SRSF5* mRNA expression, leading to decreased abundance of these splice factors and reduced availability to bind to components of the early (U1/U2) spliceosome. The mature (U4/U6.U5) spliceosome cannot be recruited, and the double-exon-skipping alternative splicing event is avoided. Consequently, only intron 10 is spliced out, ordinal pre-mRNA processing continues, and *CD44v7/8* expression is protected. Production of CD44v7/8 internalizes HA and prevents the formation of the myofibroblast-stabilizing HA coat. The mechanism(s), by which exons 11 and 12 are differentially spliced to yield the *CD44v7* and *CD44v8* transcripts, has not been identified.

MATERIALS AND METHODS

Materials

All reagents were purchased from Sigma-Aldrich or Life Technologies and Invitrogen unless otherwise stated. Reverse transcription reagents, siRNA transfection reagents, and qRT-PCR primers and reagents were purchased from Invitrogen and Applied Biosystems. Recombinant human (rh) BMP7 was from Merck Millipore.

Cell culture

Primary human lung fibroblasts and transformed human renal PTEC (HK-2) were used in all experiments. Primary human lung fibroblasts (AG02262) were purchased from Coriell Cell Repositories (Coriell Institute for Medical Research). The cells were cultured in Dulbecco's modified Eagle'smedium (DMEM)/Ham's F12 containing 5mMglucose, 2 mML-glutamine, penicillin (100 U/ml), streptomycin (100 mg/ml), and supplemented with 10% fetal bovine serum (FBS; Biological Industries Ltd.). For experiments requiring stable expression of the minigene reporters, transformed human PTECs (CRL-2190; American Type Culture Collection) were used. PTECs were the HK-2 cell line, immortalized by transduction with HPV-16 E6/E7 genes (29), and were cultured in DMEM/Ham's F12 (Life Technologies) supplemented with 10% FBS (Sera Laboratories International Ltd.) containing 5mMglucose, 2mML-glutamine, transferrin (5 mg/ml), sodium selenite (5 ng/ml), and hydrocortisone (0.4 mg/ml) (Sigma-Aldrich). All cells were maintained at 37°C in a humidified incubator in an atmosphere of 5% CO_2, and fresh growth medium was added to the cells every 3 to 4 days until the cells were ready for experimentation. Cells were growth-arrested in serum free medium for 48 hours before use in all experiments, and all experiments were performed under serum-free conditions unless otherwise stated. All experiments using fibroblasts were undertaken using cells at passage 6 to 10. Fibroblasts and PTECs (HK-2s) were stimulated with BMP7 (400 ng/ml) for 72 hours according to previous protocols (3).

Bichromatic pRG6 minigene reporter design and generation of stable cell lines

The pRG6-CD44v7 and pRG6-CD44v8 plasmids were derived from the pRG6-FGFR2 minigene plasmid (30). CD44 exon 11 (v7) or CD44 exon 12 (v8), together with corresponding upstream and downstream introns, was amplified from genomic DNA (gDNA) using specific primers and introduced into the plasmids at the XbaI/AgeI cloning sites using In-Fusion HD Cloning kits (Clontech, Takara Bio), according to the manufacturer's protocol. Two plasmid were generated: pRG6-CD44v7 and pRG6-CD44v8. Plasmids were transfected into PTECs (HK-2s) using Lipofectamine LTX reagent, according to protocol (Invitrogen). After confluence, cells were lifted with a 0.1% EDTA solution and flow-sorted, gated on EGFP expression, into fresh cultures dishes using an LSRFortessa cell sorter (BD Biosciences). Specific primer pairs were designed and purchased (Applied Biosystems) to amplify between the artificial start exon of pRG6 and the EGFP domain to confirm minigene function (see fig. S1). Fragments were amplified using the Phusion High-Fidelity DNA polymerase system (New England Biolabs). Briefly, 4 ml of 5Å~High-Fidelity buffer, 0.4 ml of deoxynucleotide triphosphate mix, 1 ml of 10 mM forward primer, 1 ml of 10 mM reverse primer, 0.2 ml of Phusion DNA polymerase, 10 ng of cDNA template, and distilled H_2O were added to a final volume of 20 ml. Samples were PCR-amplified with the following thermocycling conditions: 98°C for 30 s, 35 cycles of 98°C for 10 s, 65°C for 30 s, and 72°C for 30 s. This was followed by a final extension at 72°C for 10 min. The resultant PCR products were run on 1% agarose gels by flatbed electrophoresis. These sub-line cultures were grown to confluence and flow-sorted once more to ensure cell cultures with stable expression of each plasmid (pRG6-CD44v7 and pRG6-CD44v8). Stable cell sub-lines were grown on eight-well glass chamber slides and were fixed with 4% paraformaldehyde after treatment and mounted for visualization using fluorescent light microscopy. Nuclei were stained using VECTASHIELD DAPI (Vector Laboratories).

Immunocytochemistry

Cells were grown to 70% confluence in eight-well glass chamber slides (Merck Millipore). The culture medium was removed, and the cells were washed with sterile phosphate-buffered saline (PBS) before fixation in 4% paraformaldehyde for 10 min at room temperature. After fixation, cells were permeabilized with 0.1% (v/v) Triton X-100 in PBS for 10 min at room temperature. Slides were blocked with 1% bovine serum albumin (BSA) for 1 hour before a further washing step with 0.1% (w/v) BSA in PBS. Subsequently, the slides were incubated with rabbit antibodies recognizing human HYAL2 primary antibody (Atlas antibodies by Sigma-Aldrich) diluted in 0.1% BSA-PBS for 2 hours at room temperature. After a further washing step, slides were incubated with goat antibodies recognizing rabbit Alexa Fluor 595–conjugated secondary antibody (Invitrogen) in 0.1% BSA-PBS for 1 hour at room temperature in the dark. Cells were then mounted and analyzed by confocal fluorescent microscopy.

siRNA transfection

Transient transfections of fibroblasts and PTECs (HK-2s) were carried out with specific siRNA nucleotides (Applied Biosystems) targeting HYAL2, SRSF2, or SRSF5 mRNAs for knockdown (siHYAL ID s427, s428; siSRSF2 ID s12729, s12730; siSRSF5 ID s12738, s12739). Transfection was carried out using Lipofectamine 2000 transfection reagent (Invitrogen) in accordance with the manufacturer's protocol, and the two siRNAs for each target were cotransfected to achieve optimal knockdown. Briefly, cells were grown to 70% confluence in antibiotic free medium in either 35-mm dishes or eight-well glass chamber slides. Transfection reagent (2% v/v) was diluted in Opti-MEM reduced growth medium (Gibco) and left to incubate for 5 min at room temperature. The specific siRNA oligonucleotides were diluted in Opti-MEM reduced growth medium to achieve a final concentration of 30 nM per siRNA. The transfection agent and siRNA mixtures were then combined and incubated at room temperature for an additional 20 min. The newly formed transfection complexes were subsequently added to the cells and were incubated at 37°C with 5%CO_2 for 24 hours in serum-free medium before experimentation. As a control, cells were transfected with negative control siRNAs (scrambled sequences that bear no homology to the human genome) (Silencer Select Negative Control No. 1 and No. 2; Applied Biosystems).

Real-time qRT-PCR

Real-time qRT-PCR was used to assess HYAL2, CD44s, CD44v7/8, SRSF2, and SRSF5 mRNA expressions. Primers and probes for these genes were either commercially available or designed (table S5) and purchased from Applied Biosystems. The cells were grown in 35-mm dishes and washed with PBS before lysis with TRI-Reagent and RNA purification according to the manufacturer's protocol. Reverse transcription was carried out using the high-capacity cDNA reverse transcription kit according to the manufacturer's protocol (Applied Biosystems). This kit uses the random primer method for initiating cDNA synthesis. As a negative control, reverse transcription was carried out with sterile H_2O replacing the RNA sample. For commercially purchased TaqMan primers and probes (Applied Biosystems), qRT-PCR was carried out using the ViiA7 real-time qPCR system from Applied Biosystems in a final volume of 20 ml per sample as follows: 1 ml of reverse transcription product, 1 ml of target gene primers and probe, 10 ml of TaqMan Fast Universal PCR MasterMix, and 8 ml of sterile RNase free water. Amplification was carried out using a cycle of 95°C for 1 s and 60°C for 20 s for 40 cycles. qRT-PCR was simultaneously performed for ribosomal RNA (18S rRNA) as a standard reference gene. For assessment of custom primer pairs, designed and purchased from Invitrogen, qRT-PCR was carried out with the ViiA7 real-time qPCR system from Applied Biosystems in a final volume of 20 ml per sample as follows: 1 ml of reverse transcription product, 0.6 ml of 10 mM target gene forward primer and 0.6 ml of 10 mM target gene reverse primer, 10 ml of Power SYBR Green Master Mix, and 7.8 ml of sterile RNase-free water. Amplification used a cycle of 95°C for 15 s and 60°C for 1 min for 40 cycles, followed by a melt-curve stage at 95°C for 15 s, 60°C for 1 min, and a final step of 95°C for 15 s. qRT-PCR was simultaneously performed for glyceraldehyde-3-phosphate dehydrogenase (GAPDH) mRNA expression (custom primers designed and purchased from Applied Biosystems) as a standard reference gene. As a negative control, qRT-PCRwas performed with sterileH_2O, replacing the cDNA sample. The comparative CT method was used for relative quantification of gene expression. The CT (threshold cycle where amplification is in the linear range of the amplification curve) for the standard reference gene (rRNA/GAPDH) was subtracted from the target gene CT to obtain the DCT. The mean DCT values for replicate samples were then calculated. The expression of the target gene in experimental samples relative to expression in control samples was then calculated using the following equation: $2^{\wedge-[DCT\ (1)\ -\ DCT\ (2)]}$, where DCT (1) is the mean DCT calculated for the experimental samples, and DCT (2) is the mean DCT calculated for the control samples. The CT values for CD44s and CD44v7/8 in the different cell types used for these experiments are shown in table S6.

Nuclear protein extraction

Nuclear extraction was performed according to the following protocol: Total cell lysate was resuspended in hypotonic buffer [20 mM tris-HCl (pH 7.4), 10mMNaCl, and 3mMMgCl_2] on ice for 15min.About 10% of NP-40 detergent was added, and samples were vortexed. Homogenate was centrifuged for 10min at 1000 rcf (relative centrifugal force) at 4°C, and the supernatant (cytoplasmic fraction) was removed and frozen for future use. The pellet was resuspended in cell extraction buffer [100mM tris-HCl (pH 7.4), 2 mM Na_3VO_4, 100mM NaCl, 1% Triton X-100, 1mM EDTA, 0.1% SDS, 1mM NaF, 0.5% deoxycholate, 20mM $Na_4P_2O_7$, and 1% protease inhibitor cocktail (PIC)] and incubated on ice for 30 min with regular mixing at 10-min intervals. Samples were centrifuged at 14,000 rcf at 4°C for 30min, and the supernatant (nuclear extract) was transferred to fresh Eppendorfs and stored at −80°C until further use.

Western blot analysis

Total protein was extracted in radioimmunoprecipitation assay (RIPA) lysis buffer containing 1% PIC, 1% phenylmethylsulfonyl fluoride (PMSF), and 1% sodium orthovanadate (Santa Cruz Biotechnology). Protein was quantified before SDS–polyacrylamide gel electrophoresis and transfer to nitrocellulose. Membranes were blocked with 5% BSA/0.5% Tween 20/PBS for 1 hour (room temperature) followed by incubation with

primary antibodies diluted in 1% BSA/0.1% Tween 20/PBS overnight at 4°C. After the washing steps, membranes were incubated in secondary antibodies targeting rabbit, mouse, or rat IgG (horseradish peroxidase conjugate) (Cell Signaling Technology; 1:5000 dilution, 1% BSA/0.1% Tween 20/PBS). Detection was performed using enhanced chemiluminescence reagent (GE Healthcare) and scanned using a C-DiGit Blot Scanner (LI-COR Biotechnology).

RNA immunoprecipitation

RIP was used to assess protein association with intronic and exonic regions of CD44 pre-mRNA. RIP followed by qRT-PCR using the high-capacity cDNA reverse transcription kit according to the manufacturer's protocol (Applied Biosystems) was used to assess associations with U1, U2, U4, and U6 snRNA. Specific custom primers were designed (see table S5) and purchased from Applied Biosystems. Cells were grown in 35-mm dishes and protein cross-linked to DNA and RNA in 0.75% v/v formaldehyde (10 min, room temperature) followed by the addition of glycine (125 mM v/v; 5 min, room temperature). Cells were harvested into 1 ml of ice-cold PBS and pelleted at 1000 rcf for 5 min before resuspension in FA lysis buffer [50 mM Hepes (pH 7.5), 140mMNaCl, 1mMEDTA (pH 8), 1% Triton X-100, 0.1% sodium deoxycholate, 0.1% SDS, 1% PIC, and 1% PMSF]. Lysates were sonicated to shear DNA to fragments of ~1200 to 1500 bp (two cycles, 15 s on/60 s off, high frequency) and centrifuged for 30 s, 5000 rcf at 4°C. Supernatant was transferred to new Eppendorf tubes, and 50 ml was removed for use as an input sample. A known volume of 25 mg of protein in RIPA buffer was immunoprecipitated (IP) using antibodies recognizing HYAL2, SRSF2, or SRSF5, linked sheep anti-rabbit Dynabeads (Invitrogen; pre-absorbed with sonicated single-stranded herring sperm DNA). IP was completed with an overnight rotating incubation at 4°C. The bead complexes were centrifuged for 1 min at 2000 rcf, and the supernatant was removed. Beads were washed with wash buffer [0.1% SDS, 1% Triton X-100, 2 mM EDTA (pH 8), 150 mM NaCl, 20mMTrizma base (pH 8)] three times and once with final wash buffer (wash buffer containing 500 mM NaCl). Protein DNA was eluted with elution buffer (1% SDS, 100 mM $NaHCO_3$) at room temperature for 1 hour with continuous rotation. For RIP analysis, nuclear extraction was performed before sonication, and the IP eluate immediately underwent RNA purification using TRI-reagent followed by DNase I treatment (according to the manufacturer's protocol; New England Biolabs) to remove gDNA contamination. qRT-PCR, using the ViiA7 real-time qPCR system from Applied Biosystems, was used to assess protein-RNA associations.

Co-immunoprecipitation

A known volume of 25 mg of protein from nuclear extracts in complete cell extraction buffer was IP using antibodies specific for HYAL2, linked to sheep anti-rabbit Dynabeads (Invitrogen). IP was completed with an overnight rotating incubation at 4°C. The bead complexes were centrifuged for 1 min at 2000 rcf, and the supernatant was removed. Beads were washed with 0.1% BSA-PBS and eluted in sample loading buffer by boiling the sample for 5 min before subsequent Western blotting or MS analysis.

Identification of putative HYAL2-interacting proteins

Co-IP eluates were loading into and run down 1.5-mm 7.5% polyacrylamide gels using 1D electrophoresis (1DE). Gel plugs were manually excised, and peptides were recovered after trypsin [6.25 ng/ml in 25 mM NH_4HCO_3, 37°C, 3 hours; sequencing grade modified trypsin from Promega digestion using a modified version of the method of Shevchenko et al. (31)]. The dried peptides were resuspended in 50% (v/v) acetonitrile in 0.1% (v/v) trifluoroacetic acid (TFA; 5 ml) for MS analysis, and a 10% aliquot was spotted onto a 384-wellMS plate. The samples were allowed to dry and were then overlaid with a-cyano-4-hydroxycinnamic acid [Sigma-Aldrich; 0.5 ml of 5 mg/ml in 50% (v/v) acetonitrile and 0.1% (v/v) TFA]. MS was performed using a 4800 matrix-assisted laser desorption/ionization (MALDI) TOF/TOF mass spectrometer (Applied Biosystems) with a 200-Hz solid-state laser operating at 355 nm. MALDI mass spectra and subsequent MS/MS spectra of the eight most abundant MALDI peaks were obtained after routine calibration. Peaks were stringently selected and were analyzed with the strongest peak first. Identification queries were performed using the MASCOT Database search engine v2.1 (Matrix Science Ltd) (Perkins et al.) (32) embedded into Global Proteome Server Explorer software v3.6 (Applied Biosystems) on the Swiss-Prot database (download date, 09 January 2013) or the TrEMBL database (download date, 28 June 2011). Searches were restricted to human taxonomy with trypsin specificity (one missed cleavage allowed), and the tolerances were set for peptide identification searches at 50 parts per million for MS. One putative ID and UniProtKB (UniProt Consortium) entry is shown for each individual gel plug taken.

In silico analysis

Intronic sequences flanking exons encoding CD44v7 (exon 11) and CD44v8 (exon 12) were screened for putative exonic splice enhancer, exonic splice silencer, and splicing factor recognition sites using ESEfinder v3.0 (Cold Spring Harbor Laboratory) and Human Splicing Finder v3.0 (Aix-Marseille University). HYAL2 protein domain prediction and motif recognition were analyzed using multiple ExPASy bioinformatics

resource portal and proteomic tools (SIB Swiss Institute of Bioinformatics) and the InterPro v59 tool (EMBL-EBI).

Statistical analysis

For all data displayed in graphs, with two independent variable groupings, two-way analysis of variance (ANOVA) was used, followed by Bonferroni's multiple comparisons and post hoc Tukey's test. Graphical data are means ± SE of three independent experiments. All data were analyzed using GraphPad Prism v6. *P ≤ 0.05, **P ≤ 0.01, and ***P ≤0.001 were considered statistically significant.

SUPPLEMENTARY MATERIALS

www.sciencesignaling.org/cgi/content/full/10/506/eaao1822/DC1
Fig. S1. Schematic and confirmation of function for pRG6-CD44v bichromatic minigene reporters.
Fig. S2. In silico analysis of intronic sequence surrounding exons 11 and 12 of CD44v7 and CD44v8.
Fig. S3. Confirmation of SRSF2 and SRSF5 knockdown by Western blot.
Fig. S4. SRSF2 RIP.
Table S1. Threshold scores for SR proteins (CD44 introns 10, 11, and 12) derived from in silico analysis.
Table S2. Threshold scores for SR proteins (CD44 exons 11 and 12) derived from in silico analysis.
Table S3. Individual protein IDs from nuclear HYAL2 coimmunoprecipitation.
Table S4. In silico analysis of HYAL2 splice factor binding site thresholds.
Table S5. Primer sequences used for qRT-PCR and RIP.
Table S6. qRT-PCR cycle threshold values for CD44s and CD44v7/8.

REFERENCES AND NOTES

1. I. A. Darby, N. Zakuan, F. Billet, A. Desmoulière, The myofibroblast, a key cell in normal and pathological tissue repair. Cell. Mol. Life Sci. 73, 1145–1157 (2016).
2. S. Meran, R. Steadman, Fibroblasts and myofibroblasts in renal fibrosis. Int. J. Exp. Pathol. 92, 158–167 (2011).
3. A. C. Midgley, L. Duggal, R. Jenkins, V. Hascall, R. Steadman, A. O. Phillips, S. Meran, Hyaluronan regulates bone morphogenetic protein-7-dependent prevention and reversal of myofibroblast phenotype. J. Biol. Chem. 290, 11218–11234 (2015).
4. J. T. Buijs, M. Petersen, G. van der Horst, G. van der Pluijm, Bone morphogenetic proteins and its receptors; therapeutic targets in cancer progression and bone metastasis? Curr. Pharm. Des. 16, 1291–1300 (2010).
5. S. Meran, D. Thomas, P. Stephens, J. Martin, T. Bowen, A. Phillips, R. Steadman, Involvement of hyaluronan in regulation of fibroblast phenotype. J. Biol. Chem. 282, 25687–25697 (2007).
6. A. Wang, C. de la Motte, M. Lauer, V. Hascall, Hyaluronan matrices in pathobiological processes. FEBS J. 278, 1412–1418 (2011).
7. L. T. Senbanjo, M. A. Chellaiah, CD44: A multifunctional cell surface adhesion receptor is a regulator of progression and metastasis of cancer cells. Front. Cell Dev. Biol. 5, 18 (2017).
8. N. Matter, P. Herrlich, H. König, Signal-dependent regulation of splicing via phosphorylation of Sam68. Nature 420, 691–695 (2002).
9. H. Jiang, R. S. Peterson, W. Wang, E. Bartnik, C. B. Knudson, W. Knudson, A requirement for the CD44 cytoplasmic domain for hyaluronan binding, pericellular matrix assembly, and receptor-mediated endocytosis in COS-7 cells. J. Biol. Chem. 277, 10531–10538 (2002).
10. A. C. Midgley, M. Rogers, M. B. Hallett, A. Clayton, T. Bowen, A. O. Phillips, R. Steadman, Transforming growth factor-b1 (TGF-b1)-stimulated fibroblast to myofibroblast differentiation is mediated by hyaluronan (HA)-facilitated epidermal growth factor receptor (EGFR) and CD44 co-localization in lipid rafts. J. Biol. Chem. 288, 14824–14838 (2013).
11. B. Chowdhury, R. Hemming, S. Hombach-Klonisch, B. Flamion, B. Triggs-Raine, Murine hyaluronidase 2 deficiency results in extracellular hyaluronan accumulation and severe cardiopulmonary dysfunction. J. Biol. Chem. 288, 520–528 (2013).
12. V. Colombaro, I. Jadot, A.-E. Declèves, V. Voisin, L. Giordano, I. Habsch, J. Malaisse, B. Flamion, N. Caron, Lack of hyaluronidases exacerbates renal post-ischemic injury, inflammation, and fibrosis. Kidney Int. 88, 61–71 (2015).
13. L. Jadin, X. Wu, H. Ding, G. I. Frost, C. Onclinx, B. Triggs-Raine, B. Flamion, Skeletal and hematological anomalies in HYAL2-deficient mice: A second type of mucopolysaccharidosis IX? FASEB J. 22, 4316–4326 (2008).
14. C. Onclinx, S. Dogne, L. Jadin, F. Andris, C. Grandfils, F. Jouret, F. Mullier, B. Flamion, Deficiency in mouse hyaluronidase 2: A new mechanism of chronic thrombotic microangiopathy. Haematologica 100, 1023–1030 (2015).
15. B. Andre, C. Duterme, K. van Moer, J. Mertens-Strijthagen, M. Jadot, B. Flamion, Hyal2 is a glycosylphosphatidylinositol-anchored, lipid raft-associated hyaluronidase. Biochem. Biophys. Res. Commun. 411, 175–179 (2011).
16. V. Vigdorovich, A. D. Miller, R. K. Strong, Ability of hyaluronidase 2 to degrade extracellular hyaluronan is not required for its function as a receptor for jaagsiekte sheep retrovirus. J. Virol. 81, 3124–3129 (2007).
17. C. Duterme, J. Mertens-Strijthagen, M. Tammi, B. Flamion, Two novel functions of hyaluronidase-2 (Hyal2)

are formation of the glycocalyx and control of CD44-ERM interactions. J. Biol. Chem. 284, 33495–33508 (2009).
18. S.-L. Liu, F.-M. Duh, M. I. Lerman, A. D. Miller, Role of virus receptor Hyal2 in oncogenic transformation of rodent fibroblasts by sheep betaretrovirus Env proteins. J. Virol. 77, 2850–2858 (2003).
19. J. P. Orengo, D. Bundman, T. A. Cooper, A bichromatic fluorescent reporter for cell-based screens of alternative splicing. Nucleic Acids Res. 34, e148 (2006).
20. Y. Miyamoto, K. Yamada, Y. Yoneda, Importin a: A key molecule in nuclear transport and non-transport functions. J. Biochem. 160, 69–75 (2016).
21. C. C. Warzecha, S. Shen, Y. Xing, R. P. Carstens, The epithelial splicing factors ESRP1 and ESRP2 positively and negatively regulate diverse types of alternative splicing events. RNA Biol. 6, 546–562 (2009).
22. M. Ameyar-Zazoua, C. Rachez, M. Souidi, P. Robin, L. Fritsch, R. Young, N. Morozova, R. Fenouil, N. Descostes, J.-C. Andrau, J. Mathieu, A. Hamiche, S. Ait-Si-Ali, C. Muchardt, E. Bastché, A. Harel-Bellan, Argonaute proteins couple chromatin silencing to alternative splicing. Nat. Struct. Mol. Biol. 19, 998–1004 (2012).
23. S. Erkelenz, W. F. Mueller, M. S. Evans, A. Busch, K. Schöneweis, K. J. Hertel, H. Schaal, Position-dependent splicing activation and repression by SR and hnRNP proteins rely on common mechanisms. RNA 19, 96–102 (2013).
24. V. Bourguignon, B. Flamion, Respective roles of hyaluronidases 1 and 2 in endogenous hyaluronan turnover. FASEB J. 30, 2108–2114 (2016).
25. G. Lepperdinger, B. Strobl, G. Kreil, HYAL2, a human gene expressed in many cells, encodes a lysosomal hyaluronidase with a novel type of specificity. J. Biol. Chem. 273, 22466–22470 (1998).
26. L. Y. W. Bourguignon, P. A. Singleton, F. Diedrich, R. Stern, E. Gilad, CD44 interaction with Na+-H+ exchanger (NHE1) creates acidic microenvironments leading to hyaluronidase-2 and cathepsin B activation and breast tumor cell invasion. J. Biol. Chem. 279, 26991–27007 (2004).
27. L.-J. Hsu, L. Schultz, Q. Hong, K. van Moer, J. Heath, M.-Y. Li, F.-J. Lai, S.-R. Lin, M.-H. Lee, C.-P. Lo, Y.-S. Lin, S.-T. Chen, N.-S. Chang, Transforming growth factor b1 signaling via interaction with cell surface Hyal-2 and recruitment of WWOX/WOX1. J. Biol. Chem. 284, 16049–16059 (2009).
28. Z. Zhou, X.-D. Fu, Regulation of splicing by SR proteins and SR protein-specific kinases. Chromosoma 122, 191–207 (2013).
29. M. J. Ryan, G. Johnson, J. Kirk, S. M. Fuerstenberg, R. A. Zager, B. Torok-Storb, HK-2: An immortalized proximal tubule epithelial cell line from normal adult human kidney. Kidney Int. 45, 48–57 (1994).
30. S. Oltean, B. S. Sorg, T. Albrecht, V. I. Bonano, R. M. Brazas, M. W. Dewhirst, M. A. Garcia-Blanco, Alternative inclusion of fibroblast growth factor receptor 2 exon IIIc in Dunning prostate tumors reveals unexpected epithelial mesenchymal plasticity. Proc. Natl. Acad. Sci. U.S.A. 103, 14116–14121 (2006).
31. A. Shevchenko, O. N. Jensen, A. V. Podtelejnikov, F. Sagliocco, M. Wilm, O. Vorm, P. Mortensen, A. Shevchenko, H. Boucherie, M. Mann, Linking genome and proteome by mass spectrometry: Large-scale identification of yeast proteins from two dimensional gels. Proc. Natl. Acad. Sci. U.S.A. 93, 14440–14445 (1996).
32. D. N. Perkins, D. J. C. Pappin, D. M. Creasy, J. S. Cottrell, Probability-based protein identification by searching sequence databases using mass spectrometry data. Electrophoresis 20, 3551–3567 (1999).

Acknowledgments: We thank I. Brewis for assistance with MS and D. Gillespie for advice on statistical analyses. Funding: This work was funded by the Medical Research Council (council grant reference, MR/K010328/1).
Author contributions: A.C.M. designed and performed the experiments, developed the minigene constructs, and analyzed the data. S.O. provided expertise on alternative splicing mechanisms and provided the original minigene reporter backbones. E.L.W. designed the CD44v primers used for qRT-PCR analysis and gathered data for CD44s expression. V.H., R.S., and A.O.P. provided specialist expertise in the area and were involved in project direction and review of written manuscript. S.M. led project direction, designed the experiments, and wrote the manuscript.
Competing interests: The authors declare that they have no competing interests.

Submitted 22 June 2017
Accepted 4 October 2017
Published 21 November 2017
DOI: 10.1126/scisignal.aao1822

Citation: A. C. Midgley, S. Oltean, V. Hascall, E. L. Woods, R. Steadman, A. O. Phillips, S. Meran, Nuclear hyaluronidase 2 drives alternative splicing of CD44 pre-mRNA to determine profibrotic or antifibrotic cell phenotype. Sci. Signal. 10, eaao1822 (2017).